VIP Biosensors Very Important Paper

DOI: 10.1002/anie.201410573

# Live-cell MRI with Xenon Hyper-CEST Biosensors Targeted to Metabolically Labeled Cell-Surface Glycans**

*Christopher Witte, Vera Martos, Honor May Rose, Stefan Reinke, Stefan Klippel, Leif Schröder,* and Christian P. R. Hackenberger**

***Abstract:*** *The targeting of metabolically labeled glycans with conventional MRI contrast agents has proved elusive. In this work, which further expands the utility of xenon Hyper-CEST biosensors in cell experiments, we present the first successful molecular imaging of such glycans using MRI. Xenon Hyper-CEST biosensors are a novel class of MRI contrast agents with very high sensitivity. We designed a multimodal biosensor for both fluorescent and xenon MRI detection that is targeted to metabolically labeled sialic acid through bioorthogonal chemistry. Through the use of a state of the art live-cell bioreactor, it was demonstrated that xenon MRI biosensors can be used to image cell-surface glycans at nanomolar concentrations.*

Glycans play key roles in many biological and pathological processes, such as cell–cell interactions, virus–host interactions, embryo development, cancer cell metastasis, and immune function.[1–4] A popular method for observing changes to the glycome in living organisms is through fluorescent probes targeted to metabolically labeled glycans by using bioorthogonal chemistry.[4] These chemical tools have the potential to extend our understanding of systems biology and give insight into a variety of pathological states.[1,2] In addition, they have been successfully used not only in cells but also in vivo in transparent organisms such as zebrafish embryos.[5,6] These results have also been translated to larger opaque organisms, namely mice, but owing to the limited penetration depth of optical detection, this was limited to superficial tissue.[7] The development of magnetic resonance imaging (MRI) probes targeted to metabolically labeled glycans would overcome this problem and facilitate the non-invasive examination of such glycans in mammalian disease models. Some MRI contrast agents have been developed to target specific endogenous glycans[8,9] but to date, despite numerous attempts, MRI of metabolically labeled glycans has been unsuccessful.[7,9] Early attempts successfully confirmed targeting of conventional MRI contrast agents to metabolically labeled glycans but only indirectly through fluorescence,[10] presumably as a result of poor MRI contrast. In addition, more recent attempts in vivo and with cells were also unsuccessful.[7] The lack of successful published results over many years has even led some to question whether the imaging of metabolically labeled glycans could ever be achieved with MRI.[9] Given this, we investigated whether the unique attributes of $^{129}$Xe Hyper-CEST biosensors could address this gap in the capabilities of MRI and enable the imaging of metabolically labeled glycans in cell experiments.

Xenon Hyper-CEST biosensors[11,12] transiently and reversibly bind xenon and confer a large change in chemical shift upon binding, thus allowing bound and unbound xenon to be distinguished. Two techniques are used to amplify the signal from xenon biosensors, namely hyperpolarization and chemical exchange saturation transfer (CEST). Hyperpolarization increases the detectable signal from xenon by several orders of magnitude and has been used for the imaging of void spaces in the human lung[13] and highly perfused organs such as the rodent brain.[14,15] CEST is a detection technique that uses the reversible binding of xenon to the host to greatly amplify the signal from dilute biosensors. By using CEST, the biosensor signal can be switched on and off at will and can be acquired simultaneously with proton MRI anatomical reference images. When combined as Hyper-CEST,[12] this technique enables the imaging of xenon biosensors at very low concentrations.[16,17]

Although in vivo applications of xenon Hyper-CEST biosensors are still on the horizon, their development has culminated in several recent reports demonstrating MRI of targeted xenon biosensors in cells.[16–18] However, as one would expect in an emerging field, initial studies have focused on improving the sensitivity for biological targets that can already be addressed with conventional contrast agents. As a result, the question still remains as to whether this technology can be used to interrogate specific molecular targets that are beyond those already addressed using proton

[*] Dr. C. Witte,[+] Dr. H. M. Rose, S. Klippel, Dr. L. Schröder
ERC Project Biosensor Imaging
Leibniz-Institut für Molekulare Pharmakologie, Berlin (Germany)
E-mail: lschroeder@fmp-berlin.de
Dr. V. Martos,[+] Dr. S. Reinke, Prof. Dr. C. P. R. Hackenberger
Chemical Biology
Leibniz-Institut für Molekulare Pharmakologie, Berlin (Germany)
E-mail: hackenbe@fmp-berlin.de
Prof. Dr. C. P. R. Hackenberger
Department Chemie, Humboldt Universität zu Berlin
Berlin (Germany)
[+] These authors contributed equally to this work.

[**] This work has been supported by the European Research Council under the European Community's Seventh Framework Programme (FP7/2007-2013)/ERC grant agreement no. 242710, the Leibniz Association (WGL; grant SAW-2011-FMP-2), the Human Frontier Science Program (C. W, LT000858/2010), the DFG (SFB 765, SPP1623), the Fonds der Chemischen Industrie, the Einstein Foundation, and the Boehringer-Ingelheim Foundation (Plus 3 Award). MRI: magnetic resonance imaging, CEST: chemical exchange saturation transfer.

Supporting information for this article is available on the WWW under http://dx.doi.org/10.1002/anie.201410573.

  

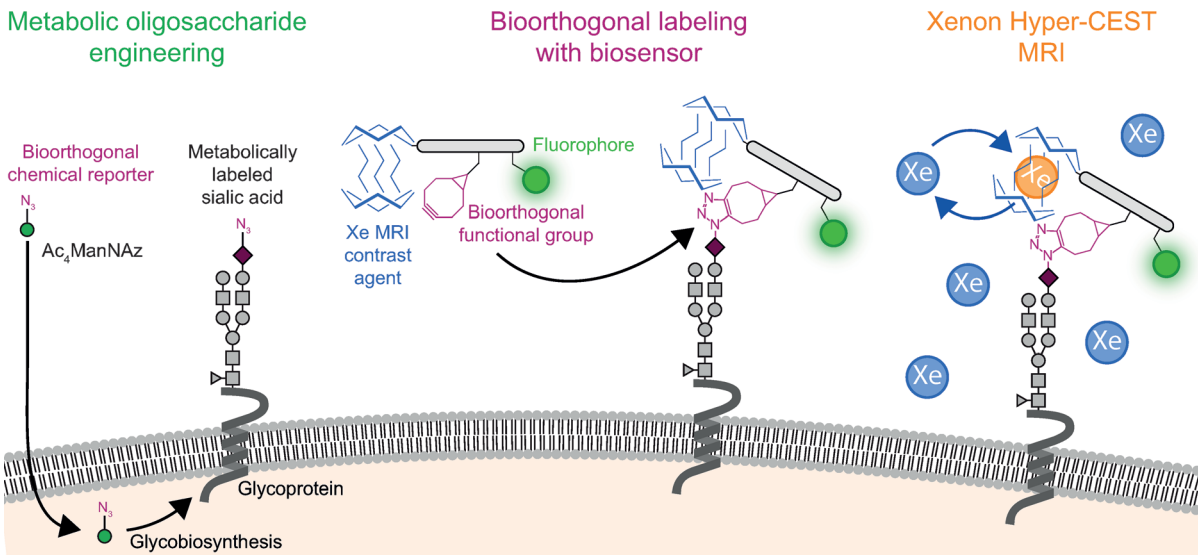


***Figure 1.*** Xenon Hyper-CEST biosensors targeted to metabolically labeled glycans using bioorthogonal chemistry. Three key steps were required to image metabolically labeled glycans on live cells with xenon Hyper-CEST biosensors. Metabolic oligosaccharide engineering (left): cells are treated with $Ac_4ManNAz$, a synthetic sugar bearing a bioorthogonal azide group, which is subsequently incorporated into the glycome as a terminal sialic acid. Bioorthogonal labeling with the biosensor (center): cells are labeled with the multimodal (xenon MRI/fluorescence) biosensor bearing a complimentary bioorthogonal functional group, xenon host, and fluorophore. Xenon Hyper-CEST MRI (right): the final step, in which hyperpolarized xenon is delivered to the sample immediately before measurement. Xenon Hyper-CEST MRI uses the reversible binding of xenon to the host to greatly amplify the biosensor signal. Of these steps, the first two could occur over the days preceding the measurement while the administration of xenon is performed immediately before the image is taken.

MRI. Herein, we show it is indeed feasible to image metabolically labeled glycans on cells using a carefully designed bioorthogonal MRI probe in combination with xenon Hyper-CEST imaging.

Three key steps were required to image metabolically labeled glycans on live cells using xenon Hyper-CEST biosensors (Figure 1). Metabolic incorporation of azides into cell-surface sialic acids using $Ac_4ManNAz$[5,6,19] was followed by bioorthogonal labeling of the resulting azidoglycans with a biosensor bearing a complementary bioorthogonal functional group and a xenon host. Finally, after the delivery of hyperpolarized xenon, the biosensor conjugates were imaged using Hyper-CEST.

We designed the multimodal biosensor **1** with three functional units (a xenon host, a bioorthogonal targeting unit, and a fluorophore; Figure 2a). Cryptophane-A (CrA) was employed as the xenon host because it has favorable properties for Hyper-CEST detection and has been used in a diverse array of biosensors.[17,18,20–24] The bioorthogonal labeling unit bicyclo[6.1.0]nonyne (BCN) was chosen because of its superior reactivity and selectivity in glycan labeling.[25] Finally, the inclusion of fluorescein permits an alternative readout to confirm selectivity and quantify biosensor uptake.[17] We decided to employ a peptide scaffold to combine these units since many methods are available, both on solid support and in solution, to produce peptides bearing multiple functional groups. Furthermore, this scaffold can be used to tune water solubility and potentially reduce nonspecific binding.[26] Previous studies,[27,28] as well as our own experience, suggested that BCN is incompatible with the required acid deprotection conditions during Fmoc-based solid-phase peptide synthesis. Therefore, to obtain biosensor **1** (Figure 2a), we developed a strategy based on the very acid-sensitive Sieber amide resin,[29] with orthogonal protecting groups and sequential modular couplings (see the Supporting Information and Figure S1 therein). The first moiety, 5,6-carboxyfluorescein, was attached on solid support after deprotection of an Alloc-protected lysine side chain. Next, the peptide was elongated and terminated with a short water-soluble PEG linker. Peptide cleavage under mild acidic conditions generated a free N terminus, to which carboxy-cryptophane-A (CrA-COOH) was coupled in solution. Finally, after acidic treatment, succinimidyl-activated BCN[30] was attached to a unique free lysine side chain. While it was employed in this study for targeting metabolically labeled sialic acid, biosensor **1** could also be used to detect a wide variety of bioorthogonal azide-labeled targets beyond glycans.[2,19,30]

Flow cytometry analysis (Figure 2b) demonstrated that biosensor **1** is specific and can successfully distinguish between cells treated with $Ac_4ManNAz$ and control cells, even in the presence of a small amount of nonspecific binding, while retaining high cell viability (> 90%; Table S1 in the Supporting Information). Triplicate measurements (Figure 2c) revealed that the median fluorescence was 4–5 times higher in the target cells than in the control cells. The observed plasma membrane staining (fluorescence microscopy, white arrow in Figure 3j) is consistent with other studies of hydrophilic BCN derivatives[25,26] and contrasts with the overall lower and punctuated staining (suggestive of nonspecific uptake) seen in the control cells (Figure 3b,e). Furthermore, since both CrA[31] and BCN[26] are known to cause unspecific binding, we investigated the effect of these units on biosensor specificity. Conjugates **2**–**4** (Figure 2a)

  

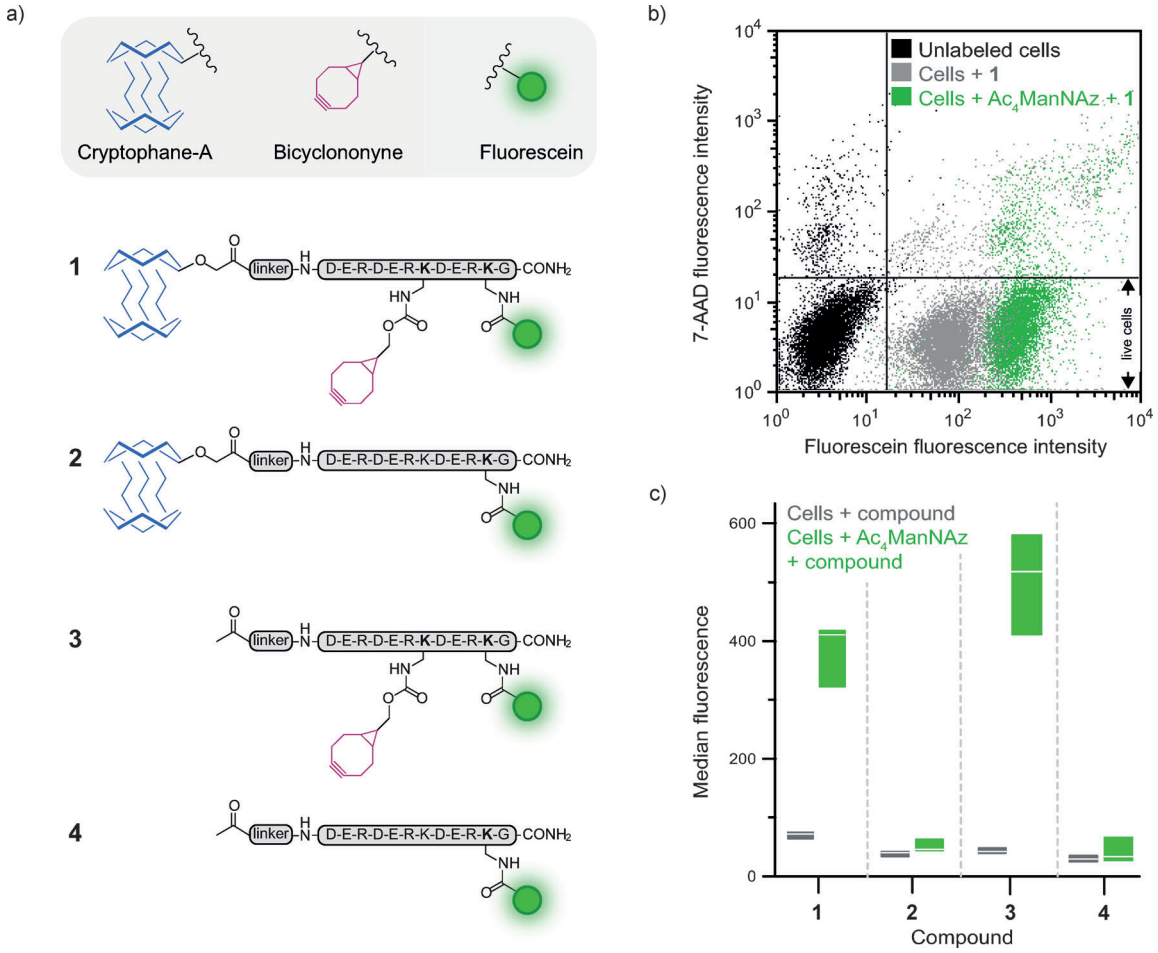


***Figure 2.*** a) Constructs **1**–**4** bearing the xenon host cryptophane-A, bicyclononyne, and fluorescein. b) Flow cytometry analysis shows the binding of biosensor **1** (measured by fluorescein fluorescence) and cell viability (measured by using the viability dye 7-Aminoactinomycin D (7-AAD)) in control cells (gray) and $Ac_4$ManNAz-treated cells (green) after 30 min incubation with biosensor **1** (50 μM, 37 °C). Untreated cells are shown in black for comparison. c) Median fluorescence intensity from flow cytometry measurements of both control cells (gray) and $Ac_4$ManNAz-treated cells (green) after incubation with constructs **1**–**4** for 30 min (50 μM, 37 °C). Results are shown for triplicate experiments; the median is indicated by a white line and the range denotes the first and third quartile.

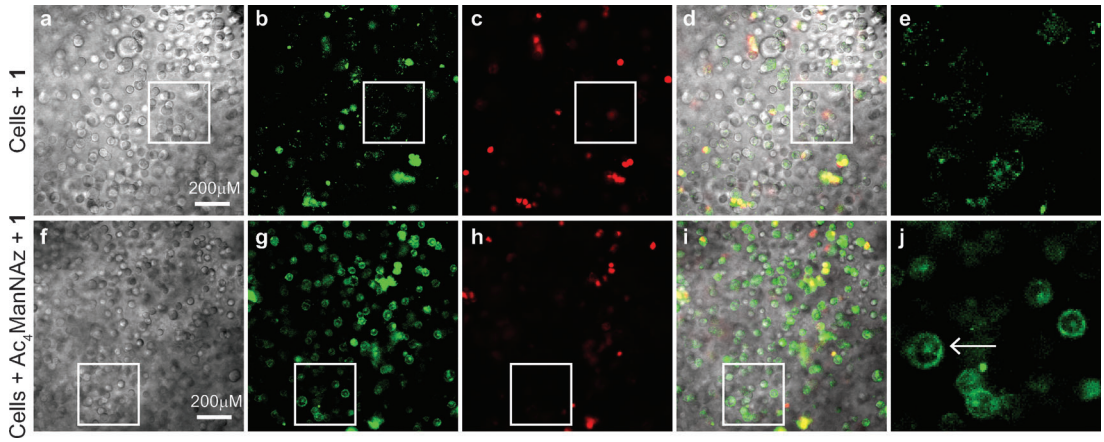


***Figure 3.*** Cells were incubated with **1** and embedded in alginate beads at ca. 10 million cells per ml. The images display a region within a single alginate bead containing many individual cells. a, f) Confocal microscopy transmission images. Fluorescence images confirm good specificity of **1** for the $Ac_4$ManNAz-treated cells [(b) and (g); detected through fluorescein, green] and high cell viability [(c) and (h); dead cells stained with ethidium homodimer III, red]. d, i) Merge of transmission and fluorescence channels. Although there is only a small percentage of dead cells, these contribute disproportionately to the unspecific binding (Table S1), presumably owing to loss of membrane integrity. e, j) magnifications of panels (b) and (g), respectively, as indicated by the white box.

were synthesized in a manner analogous to that used to produce **1** but without the attachment of BCN (**2**), CrA (**3**), or both (**4**). Each functional unit mildly increased the unspecific binding (Figure 2c), however, the BCN targeting unit confers sufficient specificity that target cells could still be easily distinguished from control cells.

We performed preliminary xenon Hyper-CEST measurements in a direct bubbling phantom (Figure S9). Such a high throughput method can be used to quickly determine whether the biosensor generates sufficient contrast, albeit at the expense of cell viability, prior to more sophisticated measurements in a live-cell bioreactor. With this setup, we correctly localized the $Ac_4$ManNAz-treated cells and confirmed the ability of xenon Hyper-CEST MRI to image metabolically labeled glycans (Figure S9c). By measuring fluorescence, we quantified the effective NMR concentration of biosensor **1** in the compartment with labeled cells as approximately 120 nM, compared to approximately 40 nM in the compartment with control cells (Figure S2 and Table S2). These values are in line with the flow cytometry data (Figure 2c) and demonstrate the exquisite sensitivity of xenon Hyper-CEST biosensors.

The results were confirmed using our previously developed bioreactor for live-cell imaging (Figure 4).[31] Delivering media presaturated with hyperpolarized xenon (Figure 4a) ensures high cell viability throughout the measurement and somewhat simulates the in vivo delivery of xenon to tissue structures.[31] It can thus be considered the system for xenon biosensors that so far comes closest to in vivo conditions. As seen in Figure 4b, the reading volume is separated into two compartments along the direction of media flow, with the cells encapsulated in alginate beads to immobilize them. Cells treated with both $Ac_4$ManNAz and biosensor **1** (Figure 4b, yellow) and control cells only treated with **1** (Figure 4b, red) are encapsulated at similar cell densities (Figure 3a,f) and placed into the separate compartments within the reading volume. The $Ac_4$ManNAz-treated cells were successfully localized through the large Hyper-CEST effect to the correct compartment (Figure 4c). This unambiguously demonstrates that xenon Hyper-CEST biosensors can be used to image metabolically-labeled cell-surface glycans on live cells. Encouragingly this can be achieved even in the presence of a degree of non-specific binding.

In summary, our work introduces a bioorthogonal Hyper-CEST xenon biosensor for imaging metabolically labeled glycans on live cells. We have thus expanded the MRI toolbox to include the imaging of glycome targets that have been difficult to investigate with conventional proton MRI contrast agents. Future work beyond this proof of principle study could include employing this biosensor to image other biomolecules carrying an azido bioorthogonal chemical reporter, for example, proteins, lipids, or cell-surface glycans other than sialic acids.[2,19,30] While sialic acid is one of the more abundant glycans,[8] a combination of already available optimizations, such as improved xenon polarization, higher xenon gas fractions, the use of isotopically enriched xenon and, in particular, the use of scaffold-based biosensors with hundreds to thousands of CEST sites,[17,18,22] will enable the investigation of rarer targets. Furthermore, since different xenon biosensors have distinct chemical shifts,[11,16,32] multiple specific molecular targets could be identified at the same time,[16,33] thereby enabling, for example, the simultaneous imaging of distinct classes of glycans, as recently demonstrated with fluorescent bioorthogonal probes.[34] Finally, given the promising pharmacokinetic modeling of xenon biosensors with a view to future applications in vivo,[16] the next goal would be to evaluate the conditions necessary to translate this method to more complex systems such as isolated perfused organs and from there to in vivo studies. Given the growing interest in investigating the glycome in living animals (especially mammals) using MRI, the novel use of xenon biosensors shown herein presents an excellent test bed for moving forward with xenon biosensors as they continue to progress in vivo.

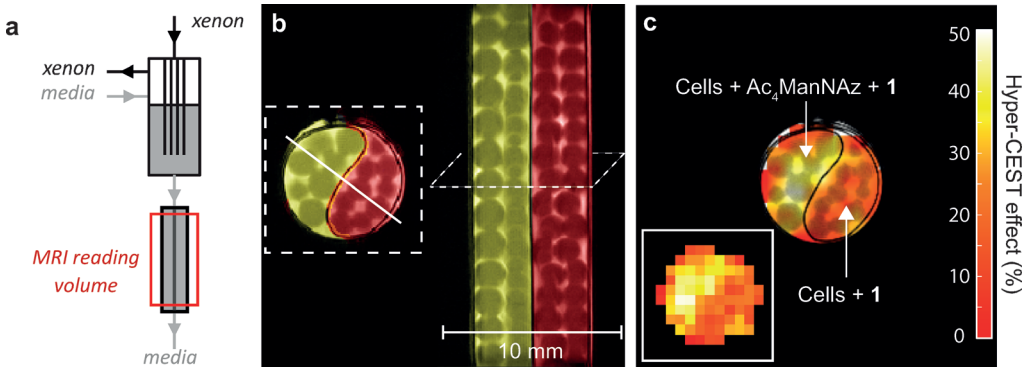


***Figure 4.*** Hyper-CEST MRI with the live cell bioreactor. a) Xenon is bubbled into media in a separate chamber and the xenon saturated medium then flows over the cells. To keep the cells fixed in the reading volume of the magnet, they are encapsulated in alginate beads. b) Proton MRI of the live cell bioreactor (digitally colored). Cells treated with both $Ac_4$ManNAz and compound **1** are located in the yellow compartment. Control cells that only receive compound **1** are located in the red compartment. c) Xenon Hyper-CEST MRI reveals the localization of the cells treated with $Ac_4$ManNAz, as determined by the higher CEST effect (yellow). The percentage CEST effect is displayed (pseudocolor) overlaid a reference proton MRI. The raw Hyper-CEST image is displayed as an insert in the lower left of the image. For the Xenon CEST images, a 30-μT 26 s saturation pulse was used, with 10 averages for each on- and off-resonant image. The dotted line in (b) indicates slice orientation for the xenon images (slice thickness = 20 mm, matrix size = 32 × 32, in-plane resolution = 625 × 625 μm$^2$, FOV = 20 × 20 mm$^2$).

Received: October 29, 2014
Revised: December 11, 2014
Published online: February 9, 2015

**Keywords:** bioorthogonal labeling · biosensors · glycosylation · host–guest systems · xenon

[1] D. H. Dube, C. R. Bertozzi, *Nat. Rev. Drug Discovery* **2005**, *4*, 477 – 488.
[2] J. A. Prescher, C. R. Bertozzi, *Nat. Chem. Biol.* **2005**, *1*, 13 – 21.
[3] C. T. Campbell, S.-G. Sampathkumar, K. J. Yarema, *Mol. BioSyst.* **2007**, *3*, 187 – 194.
[4] S. T. Laughlin, C. R. Bertozzi, *Proc. Natl. Acad. Sci. USA* **2009**, *106*, 12 – 17.
[5] S. T. Laughlin, J. M. Baskin, S. L. Amacher, C. R. Bertozzi, *Science* **2008**, *320*, 664 – 667.
[6] H. Möller, V. Böhrsch, J. Bentrop, J. Bender, S. Hinderlich, C. P. R. Hackenberger, *Angew. Chem. Int. Ed.* **2012**, *51*, 5986 – 5990; *Angew. Chem.* **2012**, *124*, 6088 – 6092.
[7] A. A. Neves, H. Stöckmann, Y. A. Wainman, J. C.-H. Kuo, S. Fawcett, F. J. Leeper, K. M. Brindle, *Bioconjugate Chem.* **2013**, *24*, 934 – 941.
[8] S. Geninatti Crich, D. Alberti, I. Szabo, S. Aime, K. Djanashvili, *Angew. Chem. Int. Ed.* **2013**, *52*, 1161 – 1164; *Angew. Chem.* **2013**, *125*, 1199 – 1202.
[9] L. Cipolla, M. Gregori, P.-W. So, *Curr. Med. Chem.* **2011**, *18*, 1002 – 1018.
[10] G. A. Lemieux, K. J. Yarema, C. L. Jacobs, C. R. Bertozzi, *J. Am. Chem. Soc.* **1999**, *121*, 4278 – 4279.
[11] M. M. Spence, E. J. Ruiz, S. M. Rubin, T. J. Lowery, N. Winssinger, P. G. Schultz, D. E. Wemmer, A. Pines, *J. Am. Chem. Soc.* **2004**, *126*, 15287 – 15294.
[12] L. Schröder, T. J. Lowery, C. Hilty, D. E. Wemmer, A. Pines, *Science* **2006**, *314*, 446 – 449.
[13] J. P. Mugler, T. A. Altes, *J. Magn. Reson. Imaging* **2013**, *37*, 313 – 331.
[14] X. Zhou, Y. Sun, M. Mazzanti, N. Henninger, J. Mansour, M. Fisher, M. Albert, *NMR Biomed.* **2011**, *24*, 170 – 175.
[15] G. Duhamel, P. Choquet, E. Grillon, L. Lamalle, J.-L. Leviel, A. Ziegler, A. Constantinesco, *Magn. Reson. Med.* **2001**, *46*, 208 – 212.
[16] M. G. Shapiro, R. M. Ramirez, L. J. Sperling, G. Sun, J. Sun, A. Pines, D. V. Schaffer, V. S. Bajaj, *Nat. Chem.* **2014**, *6*, 629 – 634.
[17] H. M. Rose, C. Witte, F. Rossella, S. Klippel, C. Freund, L. Schröder, *Proc. Natl. Acad. Sci. USA* **2014**, *111*, 11697 – 11702.
[18] M. Schnurr, K. Sydow, H. M. Rose, M. Dathe, L. Schröder, *Adv. Healthcare Mater.* **2015**, *4*, 40 – 45.
[19] J. Du, M. A. Meledeo, Z. Wang, H. S. Khanna, V. D. P. Paruchuri, K. J. Yarema, *Glycobiology* **2009**, *19*, 1382 – 1401.
[20] G. K. Seward, Y. Bai, N. S. Khan, I. J. Dmochowski, *Chem. Sci.* **2011**, *2*, 1103.
[21] Q. Wei, G. K. Seward, P. A. Hill, B. Patton, I. E. Dimitrov, N. N. Kuzma, I. J. Dmochowski, *J. Am. Chem. Soc.* **2006**, *128*, 13274 – 13283.
[22] K. K. Palaniappan, R. M. Ramirez, V. S. Bajaj, D. E. Wemmer, A. Pines, M. B. Francis, *Angew. Chem. Int. Ed.* **2013**, *52*, 4849 – 4853; *Angew. Chem.* **2013**, *125*, 4949 – 4953.
[23] M. Schnurr, C. Witte, L. Schröder, *Phys. Chem. Chem. Phys.* **2013**, *15*, 14178 – 14181.
[24] N. Tassali, N. Kotera, C. Boutin, E. L'eonce, Y. Boulard, B. Rousseau, E. Dubost, F. Taran, T. Brotin, J.-P. Dutasta, P. Berthault, *Anal. Chem.* **2014**, *86*, 1783 – 1788.
[25] J. Dommerholt, S. Schmidt, R. Temming, L. J. A. Hendriks, F. P. J. T. Rutjes, J. C. M. van Hest, D. J. Lefeber, P. Friedl, F. L. van Delft, *Angew. Chem. Int. Ed.* **2010**, *49*, 9422 – 9425; *Angew. Chem.* **2010**, *122*, 9612 – 9615.
[26] E. H. P. Leunissen, M. H. L. Meuleners, J. M. M. Verkade, J. Dommerholt, J. G. J. Hoenderop, F. L. van Delft, *ChemBioChem* **2014**, *15*, 1446 – 1451.
[27] M. Shelbourne, T. Brown, A. H. El-Sagheer, T. Brown, *Chem. Commun.* **2012**, *48*, 11184 – 11186.
[28] B. Gibson, J. M. Verkade, N. S. Barta, J. C. Hodges, F. L. Van Delft, *Chimica Oggi-Chemistry Today* **2013**, *31*, 18 – 21.
[29] H. Rink, *Tetrahedron Lett.* **1987**, *28*, 3787 – 3790.
[30] K. Lang, L. Davis, S. Wallace, M. Mahesh, D. J. Cox, M. L. Blackman, J. M. Fox, J. W. Chin, *J. Am. Chem. Soc.* **2012**, *134*, 10317 – 10320.
[31] S. Klippel, J. Döpfert, J. Jayapaul, M. Kunth, F. Rossella, M. Schnurr, C. Witte, C. Freund, L. Schröder, *Angew. Chem. Int. Ed.* **2014**, *53*, 493 – 496; *Angew. Chem.* **2014**, *126*, 503 – 506.
[32] T. K. Stevens, R. M. Ramirez, A. Pines, *J. Am. Chem. Soc.* **2013**, *135*, 9576 – 9579.
[33] S. Klippel, C. Freund, L. Schröder, *Nano Lett.* **2014**, *14*, 5721 – 5726.
[34] J. M. Baskin, K. W. Dehnert, S. T. Laughlin, S. L. Amacher, C. R. Bertozzi, *Proc. Natl. Acad. Sci. USA* **2010**, *107*, 10360 – 10365.

  